Ultrasonically Acid-assisted Milled Cellulose Nanocrystal Incorporated with TiO_2 for UV Shielding Application

Russameeruk Noonuruk [1,*], Chakkaphan Wattanawikkam [1], Weerachon Phoohinkong[2] and Kittiya Plermjai[3]

[1] *Division of Physics, Faculty of Science and Technology, Rajamagala University of Technology Thanyaburi, Pathum Thani 12110, Thailand*

[2]*Faculty of Science and Technology, Suan Dusit University, Bangkok 10700, Thailand*

[3]*Department of Science Service,75/7 Rama VI, Ratchathewi, Bangkok 10400, Thailand*

Received: 20 October 2021, Revised: 28 December 2021, Accepted:29 December 2021

Abstract

Cellulose nanocrystal (CNC) was prepared by a unique acid-assisted ultrasonically ball-milling process. XRD results affirmed that CNC product after milling process was in cellulose I_β structure, while TEM image distinctly showed cellulose nanocrystal features. CNC/TiO_2 composite was prepared by conventional mixing method using distilled water as a medium. Surface interactions between CNC and TiO_2 in the composite were investigated by XPS and FTIR spectra. CNC/TiO_2 composite was blended in polylactic acid (PLA) matrix by casting in thin layered film using a twin-screw extruder cast machine. Moreover, UV absorption performance of CNC/TiO_2 composite in PLA film was evaluated by UV-Vis spectroscopy and compared with bare PLA, TiO_2 particles and CNC in PLA film. UV absorption properties of CNC/TiO_2/PLA composite film can significantly enhanced by the incorporation of CNC and TiO_2 in PLA matrix.

Keywords: Cellulose nanocrystal, CNC/TiO_2 composite, PLA film, UV absorption

1. Introduction

Cellulose, the main part of the plant cell wall, is a polysaccharide consisting of long chains and linked by 1- 4 glycosidic bonds [1]. The hydroxyl groups in cellulose play an important role in physical properties [2]. The cellulose molecules consist of both amorphous and crystalline regions connected by hydrogen bonding between the molecules [3]. There are various sources of cellulose from plants such as bamboo, sugarcane bagasse, cotton, and wheat straw. In sugar production process, sugarcane bagasse is generated as a by-product. Meanwhile, high content of cellulose about 40-50% can be founded in sugarcane bagasse thus cellulose nanocrystal was considered and extracted from sugarcane bagasse [4]. For cellulose modification in nano-scale, surface-active area greatly increases relating to the improvement of mechanical and optical properties as flexibility and high UV absorption in UVC range [5]. Guo et al. revealed that NFC (nanofibrillated cellulose) had a good UV-shielding property, which the unmodified hand cream containing 10 wt% lignin-TiO_2 @NFC could absorb approximately 90% of UV light [6]. Meanwhile, metal oxide materials such as ZnO and TiO_2 have been practically utilized for UV shielding applications [7]. TiO_2 nanoparticles are a one of attractive materials owing to wide optical band gap, strong ultraviolet absorptivity, non-toxicity and good photocatalyst material [8]. Polylactic acid (PLA) is one of the best characterized biodegradable polymers due to its good mechanical properties, thermal plasticity, and easy to process for films preparations [9]. However, PLA is poor crystallization rate, low crystallinity, low heat distortion temperature, and high cost. Arteaga-Ballesteros et.al. used bacterial cellulose disperse into PLA matrix because it has low cost, low density, and acceptable specific strength

Corresponding Author : russameeruk_n@rmutt.ac.th

properties [10]. Marra *et.al.* shown the degradation study of PLA is faster than PLA/TiO_2 composite [11]. In this work, cellulose nanocrystal was incorporated with TiO_2 and polylactic acid to produce a composite film for the application in transparent films in visible region and shielding in UV region. Polylactic acid (PLA) was chosen as polymer matrix due to high strength, thermal plasticity and biocompatibility. CNC/TiO_2/PLA composite films are proposed for suitable material in UV protective utilization.

2. Experimental

Cellulose nanocrystal was extracted from sugarcane bagasse as wasted agriculture by ball-milling-assisted acid hydrolysis process as described in previous work [12]. Firstly, the slurry of 1% (w/w) purified cellulose in water was processed by grinding with the acid-assisted ultrasonically ball-milling process, in which precursor to ball weight ratio was specified at 1:3. The milling process was operated at 600 rpm for 5 h with a 10% sulfuric solution. The product was filtered in distilled water until the pH became neutral. For CNC/TiO_2 composite at ratio 1:1, CNC slurry was dispersed in distilled water at room temperature using a mechanical stirring at 500 rpm for 1 h. After that, TiO_2 nanoparticles were mixed and dispersed in CNC stock and continuously stirred at 500 rpm for 1 h. The final suspension was cast onto PET substrate and dried at 50 °C for 12 h to remove water and moisture. Finally, CNC/TiO_2 powder was dispersed in polylactic acid (PLA) matrix and casted in form of composite films using twin-screw extruder cast machine.

The surface morphology of cellulose nanocrystal after acid-assisted ultrasonically milling process was monitored by scanning electron microscope (HITACHI, S4700) and transmission emission microscope (JEOL, JSM3-ARM-200F). The crystalline structure and phase identification of the cellulose composites were investigated by X-ray diffraction (Rigaku, Smart lab). The surface composition of CNC/TiO_2 composite was investigated by X-ray photoelectron spectroscopy measurement (PHI5000 VeralProbll@Ulvac-PHI, Inc, JAPAN) using AlKα at the beamline 5.3 of the Synchrotron Light Research Institute (SLRI), Nakhon Ratchasima, Thailand. The chemical constituents of cellulose, TiO_2, and the composite were investigated by Fourier Transform Infrared (FTIR) spectroscopy (Thermo Scientific Nicolet 6700). The FTIR spectra were recorded in the region between 4,000 and 400 cm^{-1}. The optical transmittance of the casted films was measured in range of 190 to 700 nm using UV-Vis spectrometer (PG, T90+).

3. Results and discussion

Surface morphologies of raw material and sugarcane bagasse with cellulose exaction were monitored using a scanning electron microscope as shown in Fig. 1. The raw material of ground sugarcane bagasse in Fig. 1(a) showed rough surface and thick layer with the cell wall, lignin, hemicellulose, cellulose and other fiber. In Fig. 1(b), the morphology of cellulose with the fine surface was revealed by alkali treatment corresponding to the removal of wax, pectin, oil, lignin and hemicellulose. Moreover, cellulose nanocrystal was obtained in smooth surface and size reduction of fibrils after the production by the acid-assisted ultrasonic ball-milling process as shown in Fig. 1(c). Meanwhile, the length of cellulose nanocrystal was identified by TEM image as presented in Fig. 1(d). The typical structure and its dimensions were approximately 160 nm in length and 17 nm in width. Therefore, uniform nano-scaled of cellulose nanocrystal by acid-assisted ultrasonic ball-milling process can be obtained as previously reported [13].

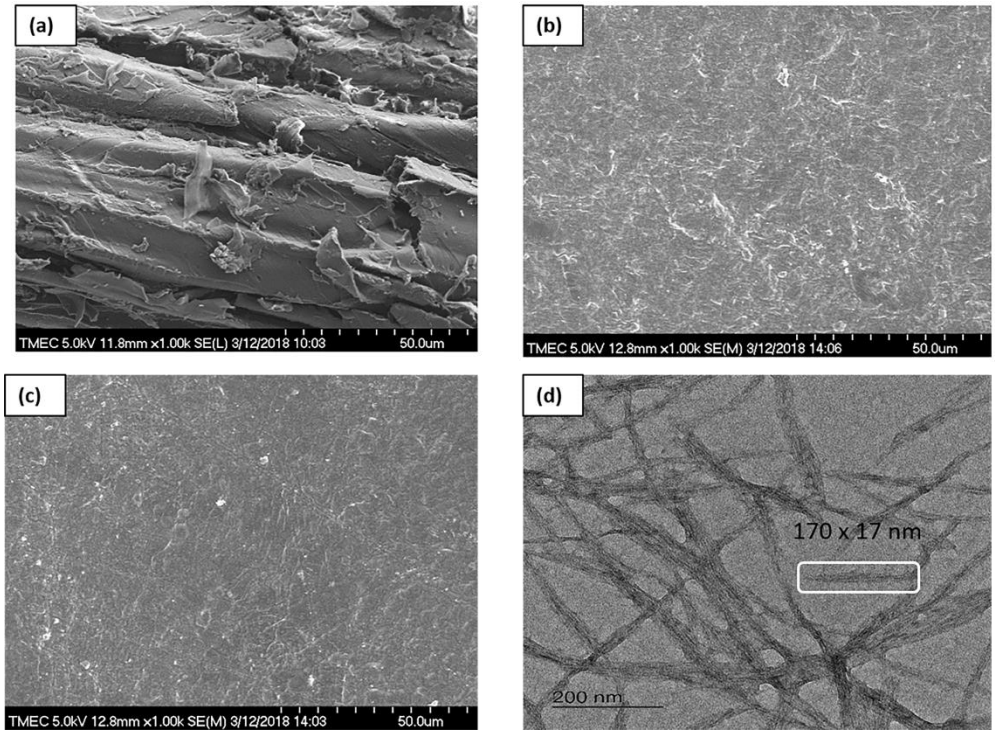

Fig. 1. SEM micrograph of (a) untreated sugarcane bagasse, (b) cellulose sample after alkali treatment, (c) cellulose nanocrystal product after acid-assisted ultrasonic ball-milling process, and (d) TEM micrograph of cellulose nanocrystal

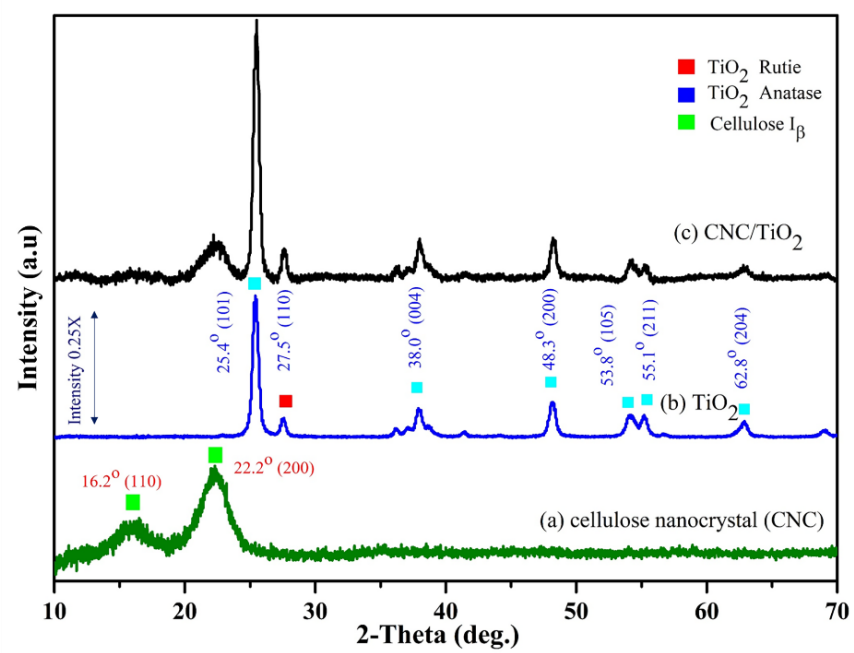

Fig. 2. XRD patterns of (a) cellulose nanocrystal, (b) TiO_2 nanoparticles, and (c) CNC/TiO_2 composite

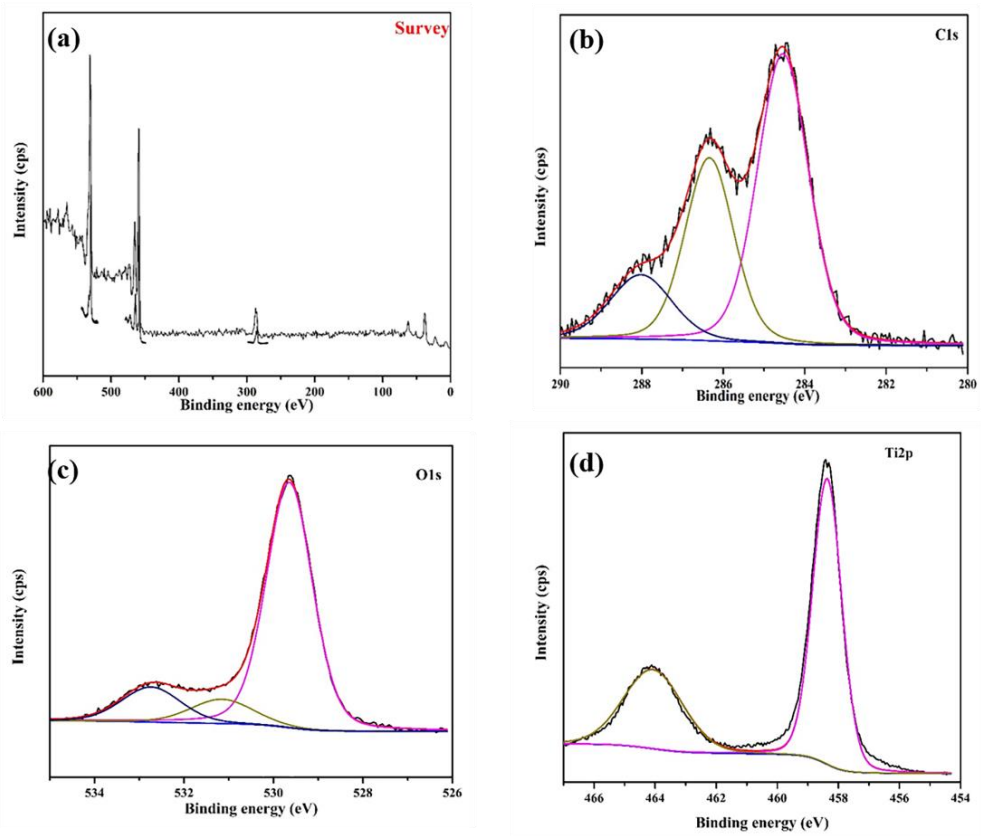

Fig. 3. XPS spectra of CNC/TiO_2 nanocomposite: (a) XPS survey spectra, high resolution of (b) C*1s* scan, (c) O*1s* scan, and (d) Ti*2p* scan

The crystalline structures with diffraction patterns of cellulose, TiO_2 and CNC/TiO_2 composite were studied using XRD measurement as shown in Fig. 2. In Fig. 2(a), two diffraction peaks located at $2\theta = 16.5^{o}$ and 22.5^{o} were characteristic of (110) and (200) planes assigned to the cellulose I_β structure in agreement with J. Guo *et al.* [14]. In Fig. 2(b), characteristic peaks located at $2\theta = 25.4°$, 38.0°, 48.3°, 53.8° and 62.8° were attributing to anatase phase of TiO_2 corresponding to (101), (004), (200), (211) and (204) planes (JCPDS 21-1272). Low-intensity peak located at 27.5° corresponded to the typical rutile phase (JCPDS 21-1276). XRD pattern of CNC/TiO_2 composite in Fig. 2(c) was identical to characteristic peaks of cellulose with I_β structure and the mixture of two polymorphs of TiO_2, in agreement with previous work of H. Han research group [15]. The results indicated that the incorporation of CNC and TiO_2 was formed in composite due to same diffraction pattern with starting materials.

The surface composition and chemical state of CNC/TiO_2 nanocomposite were investigated by using X-ray photoelectron spectroscopy (XPS) as illustrated in Fig. 3. XPS survey spectra of CNC/TiO_2 nanocomposite in Fig. 3(a) exhibited three major peaks corresponding to C*1s*, O*1s* and Ti*2p* composition. Fine scan spectra of C*1s* in Fig. 3(b) indicated three main characteristic peaks of a polysaccharide structure such as cellulose corresponding to C-C/C-H, C-O/C-OH and C-O-C component in the molecular chains at binding energy 284.8, 286.6 and 288.4 eV [15], [16], respectively. High-resolution O*1s* spectra

in Fig. 3(c) showed peak component at 529.9, 531.5, and 532.9 eV. The main peak at 529.9 eV was corresponded to O^{2-} in metal oxide lattice ascribed as Ti-O-Ti in TiO_2 crystal [17]. Meanwhile, the peak at 531.5 and 532.9 eV could be attributed to oxygen adsorbed by the hydroxyl groups on TiO_2 surface [18]. For the peak at 532.9 eV, oxygen may be combined with cellulose surface adsorbed water relating to Ti-OH bonding in the sample [17], [19]. Two peaks observed in Ti*2p* XPS spectra located at 458.7 eV and 464.4 eV were shown in Fig. 2(d). These binding energies were related to $Ti^{4+}2p_{3/2}$ and $Ti^{4+}2p_{1/2}$ of Ti^{4+} in TiO_2 lattice due to spin-orbit splitting [20], respectively. Therefore, the existence of cellulose nanocrystal and TiO_2 nanoparticles in the nanocomposite can be confirmed by the presence of C, O, and Ti XPS spectra.

FTIR spectra of PLA film, CNC/TiO_2 composite and CNC/TiO_2/PLA composite film as shown in Fig. 4. are assigned to different vibrations modes of various functional groups. Fig. 4(a) showed the characteristic peaks of PLA with the main absorption peak at 2,990, 1,452 and 1,447 cm^{-1} corresponding to CH_3 stretching vibration. The peak at 1,745 cm^{-1} indicated C=O stretching vibration mode, while the peak at 1,188 cm^{-1} is C-O-C stretching vibration [21]. In Fig. 4(b) and 4(c), the board band peak at 3,600-3,000 cm^{-1} referred to the stretching vibration of the hydroxyl groups of cellulose. The presence of C=O stretching vibration mode with the peak position at 1,757 cm^{-1} confirmed the existence of ester linkage of cellulose [22], [23]. For CNC/TiO_2/PLA composite film, it showed almost same absorption spectra as PLA matrix. These results indicated that no interaction occurred between CNC/TiO_2 nanocomposite and PLA matrix to the formation of new bonding within the composite film corresponding to same diffraction pattern of XRD result.

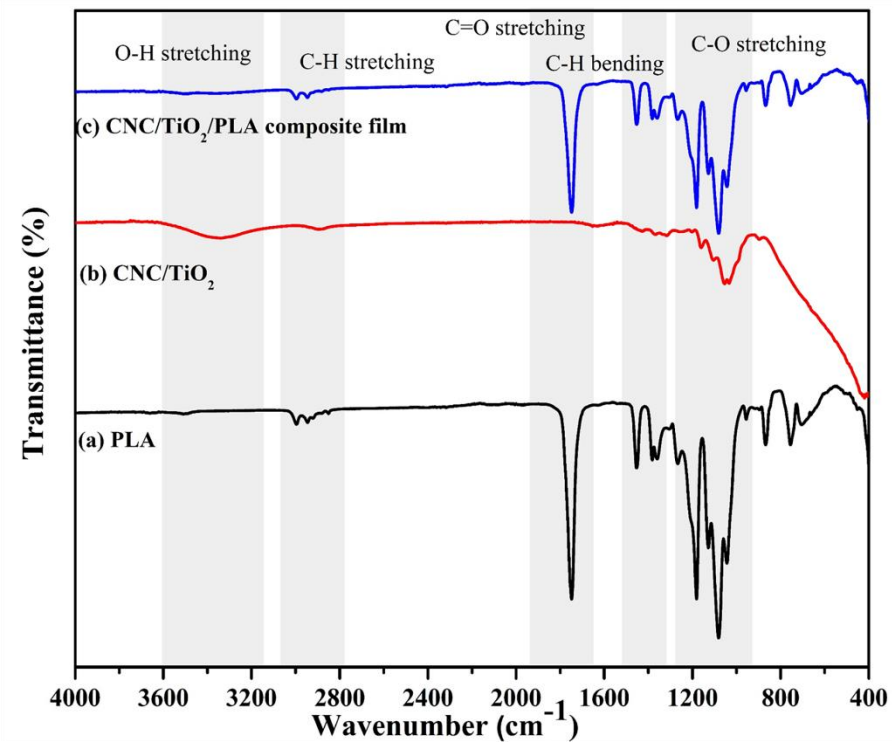

Fig. 4. FTIR spectra of (a) bare PLA film, (b) CNC/TiO_2 composite, and (c) CNC/TiO_2/PLA

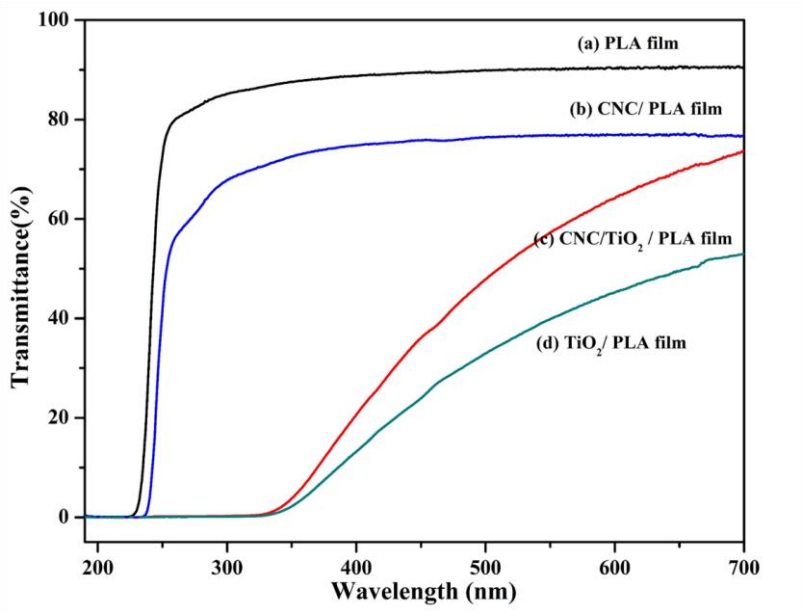

Fig. 5. Transmittance spectra of (a) PLA film, (b) CNC in PLA film, (c) CNC/TiO_2 composite in PLA film, and (d) TiO_2 in PLA film

The composite films in transmission mode were investigated using UV-vis spectroscopy in the range of 190-700 nm as shown in Fig. 5. PLA film (Fig. 5(a)) and PLA/CNC film (Fig. 5(b)) were highly transmittance above 70% in the visible region. Meanwhile, the transmittance of the composite of TiO_2/PLA film (Fig. 5(d)) in the visible region decreased because of the agglomeration of TiO_2 in the PLA matrix. On the other hand, higher transparency of CNC/TiO_2/PLA composite film was shown in Fig. 5(c) comparing with TiO_2/PLA film. This result indicated that the influence of cellulose nanocrystal is corresponded to good dispersion of TiO_2 nanoparticles in PLA matrix resulting to the improvement of film transparency. Meanwhile, high absorptions in UV region of TiO_2/PLA film and CNC/TiO_2/PLA film were strongly observed due to the influence of TiO_2 in the sample. Zeljko *et.al.* reveal that the UV-vis spectrum tends to absorb UV radiation after TiO_2 incorporated into PA coating film [24]. These results indicated that the presence of clear transparency in the visible region and high absorbance in UV region can be obtained by the incorporation of CNC and TiO_2 composite in PLA matrix.

4. Conclusion

Cellulose nanocrystal with dimension 160 nm-length and 17 nm-width was successfully prepared by acid-assisted ultrasonic ball-milling process as affirmed by SEM and TEM result. Meanwhile, CNC/TiO_2 composite was obtained by mixing surface-active process using distilled water. The existence of carbon oxygen and titanium on the sample surface was interpreted by FTIR and XPS results. For CNC/TiO_2/PLA composite films, high transparency in the visible region and strong absorbance in UV region were obviously occurred by a good distribution of TiO_2 nanoparticles accompanying with cellulose nanocrystal in PLA matrix. These results can be proposed for the application in UV shielding properties.

Acknowledgement

This work has partially been supported by Ragamangala University of Technology Thanyaburi (RMUTT) for supported the facility. For XPS experiments, authors would like to thank Synchrotron Light Research Institute (Public Organization) beamline 5.3 XPS (BL5.3: SUT−NANOTEC−SLRI).

References

[1] Teixeira EM, Bondancia TJ, Teodoro KBR, Corrêaa AC, Marconcinia JM, Mattoso LHC. Sugarcane bagasse whiskers: Extraction and characterizations. Ind. Crops Prod. 2011;33:63-6.

[2] Lin N, Huang J, Dufresne A. Preparation, properties and applications of polysaccharide nanocrystals in advanced functional nanomaterials: A review. Nanoscale 2012;4:3274-94.

[3] Moon RJ, Martini A, Nairn J, Simonsen J, Youngblood J. Cellulose nanomaterials review: structure, properties and nanocomposites. Chem. Soc. Rev. 2011;40:3941-94.

[4] Silvério HA, Neto WPF, Dantas NO, Pasquini D. Extraction and characterization of cellulose nanocrystals from corncob for application as reinforcing agent in nanocomposites. Ind. Crops Prod. 2013;44:427-36.

[5] Samir MASA, Alloin F, Dufresne A. Review of recent research into cellulosic whiskers, their properties and their application in nanocomposite field. Biomacromolecules 2005;6:612-26.

[6] Guo D, Zhang J, Sha L, Liu B, Zhang X, Zhang X, Xue G. Preparation and characterization of lignin-TiO_2 UV-shielding composite material by induced synthesis with nanofibrillated cellulose. Bioresour. 2020;15(4):7374-89.

[7] Zhang YW, Zhuang SD, Xu XY, Hu JG. Transparent and UV-shielding ZnO@PMMA nanocomposite films. Opt. Mater. 2013;36:169-72.

[8] Calvo ME, Smirnov JRC, Míguez H. Novel approaches to flexible visible transparent hybrid films for ultraviolet protection. J. Polym. Sci., Part B: Polym. Phys. 2012;50: 945-56.

[9] Tanase-Opedal M, Espinosa E, Rodríguez A, Chinga-Carrasco G. Lingin: A biopolymer from forestry biomass for bicomposites and 3D printing. Materials 2019;12:3006.

[10] Arteage-Ballesteros BE, Guevara-Morales A, Martín-Martínez ES, Figueroa-López U, Vieyra H. Composite of polylactic acid and microcellulose from kombucha membranes, e-Polymers 2021;20:15-26.

[11] Marra A, Cimmino S, Silvestre C. Effect of TiO_2 and ZnO on PLA degradation in various media. Adv. Mater Sci. 2017;2(2):2-8.

[12] Plermjai K, Boonyarattanakalin K, Mekprasart W, Pavasupree S, Phoohinkong W, Pecharapa W. Extraction and characterization of nanocellulose from sugarcane bagasse by ball milling- assisted acid hydrolysis. AIP Conf. Proc. 2018;2010:020005.

[13] Mandal A, Chakrabarty D. Isolation of nanocellulose from waste sugarcane bagasse (SCB) and its characterization. Carbohydr. Polym. 2011;86:1291-9.

[14] Plermjai K, Boonyarattanakalin K, Mekprasart W, Phoohinkong W, Pavasupree S, Pecharapa W. Optical absorption and FTIR study of cellulose/TiO_2 hybrid composite. Chiang Mai J. Sci. 2019;46:618-25.

[15] Kamarudin1 SH, Abdullah LC, Aung MM, Ratnam CT. A study of mechanical and morphological properties of PLA based biocomposites prepared with EJO vegetable oil based plasticiser and kenaf fibres. IOP Conf. Ser.: Mater. Sci. Eng. 2018;368:012011.

[16] Chauhan I, Chauhan P. In situ decoration of TiO_2 nanoparticles on the surface of cellulose fibers and study of their photocatalytic and antibacterial activities. Cellulose 2015;22:507-519.
[17] Weber F, Koller G, Schennach R, Bernt I, Eckhart R. The surface charge of regenerated cellulose fibres. Cellulose 2013;20:2719-29.
[18] Yan JQ, Wu J, Guan NJ, Li LD, Li ZX, Cao XZ. Understanding the effect of surface/bulk defects on the photocatalytic activity of TiO_2: Anatase versus rutile. Phys. Chem. Chem. Phys. 2013;15:10978-88.
[19] Tsuji E, Fukui KI, Imanishi A. Influence of surface roughening of rutile single-crystalline TiO_2 on photocatalytic activity for oxygen photoevolution from water in acidic and alkaline solutions. J. Phys. Chem. C. 2014;118:5406-13.
[20] Jackman MJ, Thomas AG, Muyn V. Photoelectron spectroscopy study of stoichiometric and reduced anatase TiO_2 (101) surfaces: the effect of subsurface defects on water adsorption at near-ambient pressures. J. Phys. Chem. C. 2015;119:13682-90.
[21] Mai TTT, Nguye TTT, Le QD, Nguyen TN, Ba TC, Nguyen HB, Phan TBH, Tran DL, Nguyen XP, Park JS. A novel nanofiber Cur-loaded polylactic acid constructed by electrospinning. Adv. Nat. Sci.: Nanosci. Nanotechnol. 2012;3:025014.
[22] Liu W, Mohanty AK, Askeland P, Drzal LT, Misra M. Influence of fiber surface treatment on properties of Indian grass fiber reinforced soy protein based biocomposites. Polymers 2004;45:7589–96.
[23] Tserki V, Zafeiropoulos NE, Simon F, Panayiotou C. A study of the effect of acetylation and propionylation surface treatments on natural fibres. Composites, Part A 2005;36: 1110-8.
[24] Zeljko M, Bulatović VO, Špada V, Blagojević SL. Environmentally friendly UV-protective polyacrylate/TiO_2 nanocoatings. Polymers 2021;13:2609.